An integral equation and its application to spiral antennas on semi-infinite dielectric materials

HIROSE, Kazuhide / NAKANO, Hisamatsu / YAMAUCHI, Junji / OHSHIMA, Ichiro

An Integral Equation and its Application to Spiral Antennas on Semi-Infinite Dielectric Materials

Hisamatsu Nakano, *Fellow, IEEE*, Kazuhide Hirose, *Member, IEEE*, Ichiro Ohshima, and Junji Yamauchi, *Member, IEEE*

Abstract— This paper presents an integral equation that can handle wire antennas on a semi-infinite dielectric material. The integral equation is reduced to a set of linear equations by the method of moments. For efficiency, the impedance matrix element $Z_{m,n}$ is divided into two parts on the basis of weighted Green's function extractions. The far-zone radiation field, which is formulated using the stationary phase method, is also described. After the validity of the presented numerical techniques is checked using a bow-tie antenna, a spiral antenna is analyzed. The current distribution, radiation pattern, axial ratio, power gain, and input impedance are discussed. It is found that the radiation field inside a dielectric material is circularly polarized. As the relative permittivity of the dielectric material increases, the angle coverage over which the axial ratio is less than 3 dB becomes narrower.

Index Terms—Millimeter-wave antennas, spiral antennas.

I. INTRODUCTION

PLANAR antennas coupled to millimeter-wave detectors have been investigated for plasma diagnostics, astronomy, and radar applications [1], [2]. These antennas and detectors are made on a hyperhemispherical lens as a monolithic integrated circuit. Since the hyperhemispherical lens is electrically large, the antennas act as if they were located on a semi-infinite dielectric material. Therefore, it is essential for us to know the radiation from the antenna into the dielectric material [3].

In the first part of this paper, an integral equation is derived for analyzing arbitrarily shaped wire antennas on a semi-infinite dielectric material, where the Hertz vector for an infinitesimal current element is expressed in reference to a cylindrical coordinate system [4]. The derived integral equation is recognized as an extended version of an equation for "wire near an interface" in [5, Sec. B.] since it can handle an arbitrary wire configuration (note that "wire near an interface" in [5] is straight). Also, the derived integral equation is recognized as a special one in the general expression for a scatterer (whose surface is approximated by triangle patches) penetrating the interface between dissimilar media [6].

The derived integral equation is transformed to a set of linear equations by applying the method of moments (MoM). The impedance matrix element $Z_{m,n}$ in the MoM, involving triple integrals (unlike quadruple integrals in the Fourier transform-domain MoM), is divided into two parts—$Z_{m,n}^{\rho}$ and

$\Delta Z_{m,n}$—for more efficient calculation. These two parts are based on the extraction of asymptotic values [7] that form weighted free-space Green's functions [8].

The radiation fields in the air and dielectric material regions are also formulated by the stationary phase method [9], [10]. The formulation is carried out in such a way that the final results formally resemble those for a printed wire on a grounded dielectric substrate [11]. This resemblance is helpful in writing the analysis computer program since the same computational flow for the printed wire on the grounded substrate can be used.

In the second part of this paper, a computer program is written on the basis of the formulation derived in this paper. After confirming the fact that the program reproduces the published data of a bow-tie antenna [12], the same computer program is applied to a spiral antenna on a semi-infinite dielectric material. Note that there have been few investigations of spirals on a semi-infinite dielectric material [2], even though investigations of spirals in various configurations have been made: spirals in free space [13], spirals backed by a plane reflector [14]–[17], spirals backed by a cavity [18], spirals in a triplate transmission line [19], and spirals on a dielectric substrate backed by a conducting plane reflector [11], [20].

This paper presents the numerical results of the spiral on the semi-infinite dielectric material together with those of a spiral antenna isolated in a homogenous medium (free space). The current distribution, radiation pattern, axial ratio, input impedance, and gain are revealed. The numerical results show that the radiation field inside the semi-infinite dielectric material is circularly polarized and that the angle coverage over which the radiation field has an axial ratio of less than 3 dB becomes narrower as the relative permittivity of semi-infinite dielectric material increases. The frequency responses of the radiation characteristics are also presented and discussed.

II. FORMULATION

A. Integral Equation

Fig. 1 shows a wire antenna of arbitrary shape. The wire (whose radius is a) is located on a semi-infinite dielectric material with permittivity ε_r. It is assumed that the dielectric material is lossless and the wire is perfectly conducting. It is also assumed that the wire radius is much less than the wavelength. This thin wire assumption ensures that the current flows only in the axial direction of the wire.
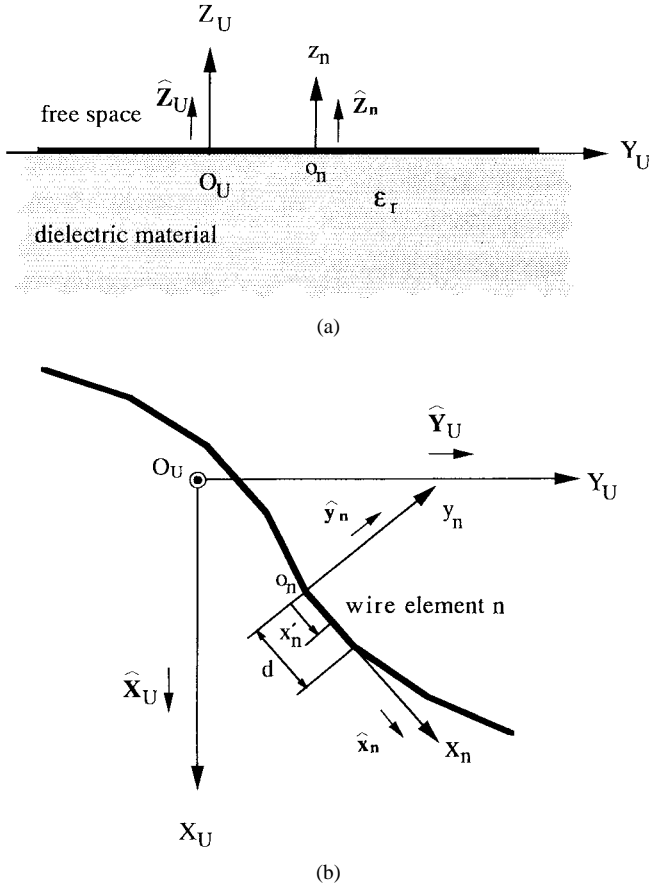
(a)

(b)

Fig. 1. A wire on a semi-infinite dielectric material.

We subdivide the wire of arbitrary shape into many elements, each being regarded as a linear element of length d. These wire elements are labeled $0, 1, 2, \cdots, i, \cdots, n - 1$, $n, \cdots, N$. Note that wire element n is handled by the nth local coordinate system, shown in Fig. 1, where the x_n coordinate is taken in such a way that it is parallel to the axis of wire element n. $\hat{\mathbf{x}}_n$, $\hat{\mathbf{y}}_n$, and $\hat{\mathbf{z}}_n$ are the unit vectors for the x_n, y_n, and z_n coordinates, respectively. Observation and source points are expressed as (x_n, y_n, z_n) and (x'_n, y'_n, z'_n) in the nth coordinate system. The rectangular coordinate system (X_u, Y_u, Z_u, O_u) in Fig. 1 is the universal coordinate system, of which the unit vectors are $\hat{\mathbf{X}}_U$, $\hat{\mathbf{Y}}_U$, and $\hat{\mathbf{Z}}_U$.

The total electric field due to the currents $I(x'_n)$ ($n = 0, 1, 2, \cdots, N$) distributed along all wire elements is obtained by summing the electric field from each wire element. The tangential component of the total electric field on wire element i has a relationship of

$$\sum_{n=0}^{N} \int_0^d \left[k_0^2 \prod_n^{(\mathrm{air})\mathrm{x}} (\hat{\mathbf{x}}_n \cdot \hat{\mathbf{x}}_i) + \frac{\partial}{\partial x'_n} \frac{\partial}{\partial x_i} G_n^{(\mathrm{air})} \right]_{z_n = 0}$$
$$\times I(x'_n) \, dx'_n = -E_{\mathrm{tan}}^{\mathrm{inc}} \qquad (1)$$

where $k_0 = \omega\sqrt{\mu_0 \varepsilon_0} \equiv k^{(\mathrm{air})}$; x_i is the x variable in the ith local coordinate system whose unit vector along the x_i coordinate is $\hat{\mathbf{x}}_i$, $E_{\mathrm{tan}}^{\mathrm{inc}}$ is the tangential component of the electric field incident or impressed on the wire surface, $G_n^{(\mathrm{air})}$ is defined as $G_n^{(\mathrm{air})} = -\prod_n^{(\mathrm{air})\mathrm{x}} + \prod_n^{(\mathrm{air})}$, where the Hertz
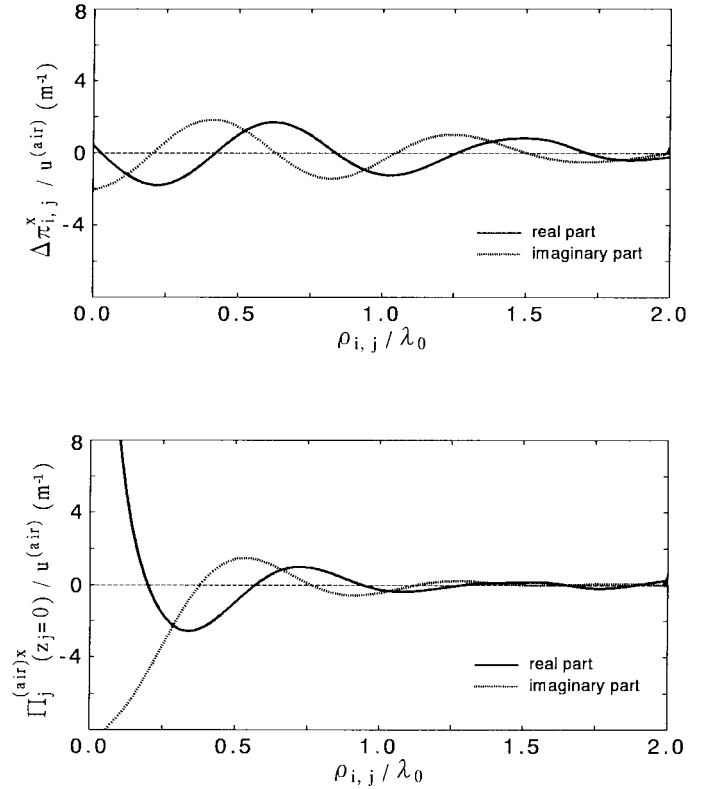
Fig. 2. $\Delta \pi_{i,j}^x$ and $\prod_j^{(\mathrm{air})\mathrm{x}} (z_j = 0)$.

vector potential functions [4] are

$$\prod_n^{(\mathrm{air})\mathrm{x}} = u^{(\mathrm{air})} \int_0^\infty J_0(\lambda\rho) \frac{\lambda}{\mu} \left[e^{-\mu|z_n|} + \frac{\mu - \mu_e}{\mu + \mu_e} e^{-\mu z_n} \right] d\lambda \qquad (2)$$

$$\prod_n^{(\mathrm{air})} = 2u^{(\mathrm{air})} \frac{1}{k_0^2} \int_0^\infty J_0(\lambda\rho) \frac{\mu - \mu_e}{(k^2/k_0^2)\mu + \mu_e} \lambda\mu e^{-\mu z_n} \, d\lambda. \qquad (3)$$

The notations in (2) and (3) are defined as $u^{(\mathrm{air})} = -j\omega\mu_0/[4\pi(k^{(\mathrm{air})})^2]$, $\mu = [\lambda^2 - (k^{(\mathrm{air})})^2]^{1/2}$, $\mu_e = [\lambda^2 - (k^{(\mathrm{die})})^2]^{1/2}$ with $k^{(\mathrm{die})} = \omega\sqrt{\mu_0\varepsilon_0\varepsilon_r} = k$, and $J_0(\lambda\rho)$ is the Bessel function of the first kind of order zero with an argument $\lambda\rho$, where ρ is the distance between observation and source points.

B. Impedance Matrix of Moment Method

The MoM is adopted for obtaining the current distribution on the wire. We expand the current $I(x'_n)$ in (1) using piecewise sinusoidal functions $I(x'_n) = I_n \sin k_0(d - x'_n)/\sin k_0 d + I_{n+1} \sin k_0 x'_n / \sin k_0 d$, $(0 \leq x'_n \leq d; n = 0, 1, 2, \cdots, N)$, where I_n and I_{n+1} are the unknown expansion coefficients to be determined (note: $I_0 = I_{N+1} = 0$). Applying weighting functions to (1) after this current expansion, we obtain a set of linear equations $[Z_{m,n}][I_n] = [V_m]$, where $[Z_{m,n}]$, $[I_n]$, and $[V_m]$ are the impedance, current, and voltage matrices, respectively, for the MoM.

The impedance matrix elements $Z_{m,n}$ in this paper are formulated using piecewise sinusoidal functions for the weighting functions (Galerkin's method). The $Z_{m,n}$ involve triple inte-

grals, which lead to less computational burden, compared with that of the impedance matrix element calculation in the Fourier transform-domain MoM (quadruple integrals). The $Z_{m,n}$ are

$$Z_{m,n} = Z^\rho_{m,n} + \Delta Z_{m,n} \qquad (4)$$

where

$$Z^\rho_{m,n} = \left(\frac{k_0}{\sin k_0 d}\right)^2 \left(g^\rho_{m-1,n-1} + g^\rho_{m-1,n}\right. \\ \left. + g^\rho_{m,n-1} + g^\rho_{m,n}\right) \qquad (5)$$

$$\Delta Z_{m,n} = \left(\frac{k_0}{\sin k_0 d}\right)^2 \left(\Delta g_{m-1,n-1} + \Delta g_{m-1,n}\right. \\ \left. + \Delta g_{m,n-1} + \Delta g_{m,n}\right). \qquad (6)$$

Note that $g^\rho_{i,j}$ $(i = m-1, m; j = n-1, n)$ in (5) are defined as

$$g^\rho_{i,j} = \eta_{m(i)} \int_0^d (\cos x_{m(i)})\left(h^{\langle 1 \rangle}_{i,j} + h^{\langle 3 \rangle}_{i,j}\right) dx_i \\ + (\hat{\mathbf{x}}_i \cdot \hat{\mathbf{x}}_j) \int_0^d (\sin x_{m(i)}) h^{\langle 2 \rangle}_{i,j} \, dx_i \qquad (7)$$

where $x_{m(i)}$ is defined as $x_{m(m-1)} = k_0 x_{m-1}$ for $i = m-1$ and $x_{m(m)} = k_0(d - x_m)$ for $i = m$. $\eta_{m(i)}$ is defined as $\eta_{m(m-1)} = 1$ for $i = m-1$ and $\eta_{m(m)} = -1$ for $i = m$. $h^{\langle 1 \rangle}_{i,j}, h^{\langle 2 \rangle}_{i,j}$, and $h^{\langle 3 \rangle}_{i,j}$ are

$$h^{\langle 1 \rangle}_{i,j} = -\eta_{n(j)} \int_0^d \pi^x_{i,j} \cos x'_{n(j)} \, dx'_j \qquad (8)$$

$$h^{\langle 2 \rangle}_{i,j} = \int_0^d \pi^x_{i,j} \sin x'_{n(j)} \, dx'_j \qquad (9)$$

$$h^{\langle 3 \rangle}_{i,j} = \eta_{n(j)} \int_0^d \pi_{i,j} \cos x'_{n(j)} \, dx'_j \qquad (10)$$

where

$$\pi^x_{i,j} = u^{(\text{air})} \frac{e^{-jk_0 \rho_{i,j}}}{\rho_{i,j}} \qquad (11)$$

$$\pi_{i,j} = u^{(\text{air})} \frac{\varepsilon_r - 1}{\varepsilon_r + 1} \frac{e^{-jk_0 \rho_{i,j}}}{\rho_{i,j}}. \qquad (12)$$

$\Delta g_{i,j}$ $(i = m-1, m; j = n-1, n)$ in (6) has the same form as $g^\rho_{i,j}$ in which $h^{\langle q \rangle}_{i,j}$ $(q = 1, 2, \text{and } 3)$ are replaced by $\Delta h^{\langle q \rangle}_{i,j}$. This replacement is accomplished by transforming $\pi^x_{i,j}$ and $\pi_{i,j}$ to $\Delta \pi^x_{i,j}$ and $\Delta \pi_{i,j}$, respectively, where

$$\Delta \pi^x_{i,j} = u^{(\text{air})} \int_0^\infty J_0(\lambda \rho_{i,j}) \left[\frac{2\mu}{\mu + \mu_e} - 1\right] \frac{\lambda}{\mu} \, d\lambda \qquad (13)$$

$$\Delta \pi_{i,j} = u^{(\text{air})} \int_0^\infty J_0(\lambda \rho_{i,j}) \frac{\lambda}{\mu} \left[\frac{2}{k_0^2} \frac{(\mu - \mu_e)\mu^2}{\varepsilon_r \mu + \mu_e} - \frac{\varepsilon_r - 1}{\varepsilon_r + 1}\right] d\lambda. \qquad (14)$$

Note that the pair of subscripts i and j indicates that the observation and source points are located on the wire elements i and j, respectively. $\rho_{i,j}$ is the distance between these two points. Equation (13) is the $\prod^{(\text{air})x}_j (z_j = 0)$ (2) from which the free-space Green's function $\pi^x_{i,j}$ is extracted. Equation (14) is the $\prod^{(\text{air})}_j (z_j = 0)$ (3) from which the weighted free-space
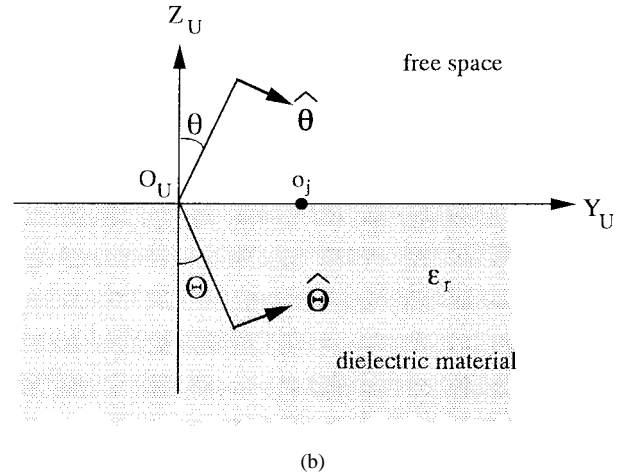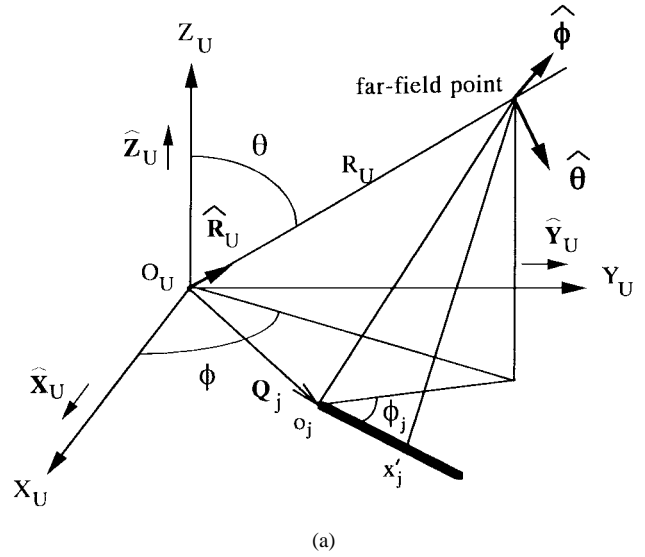

(a)

(b)

Fig. 3.   Coordinate system for radiation field formulation.

Green's function $\pi_{i,j}$ is extracted. These extractions yield values of one and $(\varepsilon_r - 1)/(\varepsilon_r + 1)$ in the square brackets within the integrands in (13) and (14), respectively.

Note that the values of one and $(\varepsilon_r - 1)/(\varepsilon_r + 1)$ are the asymptotic values of $2\mu/(\mu + \mu_e)$ and $(2/k_0^2)[(\mu - \mu_e)\mu^2]/[\varepsilon_r \mu + \mu_e]$, respectively. Therefore, the integrals for $\Delta \pi^x_{i,j}$ and $\Delta \pi_{i,j}$ quickly converge. The computing time of $\Delta \pi^x_{i,j}$ is approximately one-half of the computing time of $\prod^{(\text{air})x}_j (z_j = 0)$. A similar reduction in computing time is also found between $\Delta \pi_{i,j}$ and $\prod^{(\text{air})}_j (z_j = 0)$.

Enormous integral calculations of $\Delta \pi^x_{i,j}$ and $\Delta \pi_{i,j}$ which vary with $\rho_{i,j}$ are required for filling the impedance matrix $[Z_{m,n}]$. Fortunately, $\Delta \pi^x_{i,j}$ and $\Delta \pi_{i,j}$ show slow change with respect to $\rho_{i,j}$ since they do not contain $1/\rho_{i,j}$ dependence after the extraction operation (Fig. 2 illustrates this fact making a comparison between $\Delta \pi^x_{i,j}$ and $\prod^{(\text{air})x}_j (z_j = 0)$. As $\rho_{i,j}$ decreases toward zero, the change in $\prod^{(\text{air})x}_j (z_j = 0)$ becomes rapid). Hence, after $\Delta \pi^x_{i,j}$ and $\Delta \pi_{i,j}$ are calculated for some representative $\rho_{i,j}$, they can be interpolated with respect to $\rho_{i,j}$ instead of performing the time-consuming integral calculations. This interpolation reduces the fill time for $Z_{m,n}$.

For example, we can reduce the fill time for 11×11 matrix elements $Z_{m,n}$ by a factor of 60 using both the interpolation and asymptotic extraction techniques for a half-wave dipole on a dielectric substrate of $\varepsilon_r = 2.55$. Similar extraction and interpolation are found in the numerical analysis of a microstrip dipole antenna with a grounded dielectric substrate [7], [8].

C. Far-Zone Fields

Fig. 3 is used for calculating the electric field at a far-field point (R_U, θ, ϕ) in the spherical coordinate system whose unit vectors are $(\hat{\mathbf{R}}_U, \hat{\boldsymbol{\theta}}, \hat{\boldsymbol{\phi}})$. ϕ_j is an angle between the jth x coordinate and a line joining the jth coordinate origin o_j with the projection of the far-field point into the universal $X_U - Y_U$ plane. $\mathbf{Q}_j$ is a vector directed to the jth local coordinate origin o_j from the universal coordinate origin O_U. For simplicity, angle $\theta^{(v)}$ and relative permittivity $\varepsilon_r^{(v)}$ ($v =$ air, die) are used, which are defined as $\theta^{(\text{air})} = \theta$, $\theta^{(\text{die})} = \Theta$ ($= \pi - \theta$), $\varepsilon_r^{(\text{air})} = 1$, and $\varepsilon_r^{(\text{die})} = \varepsilon_r$.

Using the stationary phase method [9], we obtain the p component of the far-zone fields in the air and dielectric regions, $E_p^{(v)}$ ($v =$ air, die; $p = \theta, \phi$)

$$E_\theta^{(v)} = n_f^{(v)} C_\theta^{(v)} \sum_{n=1}^{N} I_n \sum_{j=n-1}^{n} \eta_{n(j)} \alpha_j^{(v)}$$
$$\cdot [-\cos\phi \hat{\mathbf{X}}_U - \sin\phi \hat{\mathbf{Y}}_U] \cdot \hat{\mathbf{x}}_j \quad (15)$$

$$E_\phi^{(v)} = n_f^{(v)} C_\phi^{(v)} \sum_{n=1}^{N} I_n \sum_{j=n-1}^{n} \eta_{n(j)} \alpha_j^{(v)}$$
$$\cdot [-\cos\phi \hat{\mathbf{Y}}_U + \sin\phi \hat{\mathbf{X}}_U] \cdot \hat{\mathbf{x}}_j \quad (16)$$

where

$$n_f^{(v)} = u^{(v)} \frac{\sqrt{\varepsilon_r^{(v)}} k^{(v)}}{\sin k_0 d} \frac{e^{-jk^{(v)} R_u}}{R_u} \quad (17)$$

(see (18) at the bottom of the page)

$$C_\phi^{(v)} = \frac{\sqrt{\varepsilon_r^{(v)}} \cos\theta^{(v)}}{\left(\sqrt{1 - \varepsilon_r^{(v)} \sin^2\theta^{(v)}} + \sqrt{\varepsilon_r - \varepsilon_r^{(v)} \sin^2\theta^{(v)}}\right)} \quad (19)$$

$$\alpha_{n-1}^{(v)} = e^{jk^{(v)} \mathbf{Q}_{n-1} \cdot \hat{\mathbf{R}}_U} \left[\frac{1}{C_{n-1}^{+(v)}} \left(e^{jk_0 d C_{n-1}^{+(v)}} - 1 \right) \right.$$
$$\left. + \frac{1}{C_{n-1}^{-(v)}} \left(e^{-jk_0 d C_{n-1}^{-(v)}} - 1 \right) \right] \quad (20)$$

$$\alpha_n^{(v)} = e^{jk^{(v)} \mathbf{Q}_n \cdot \hat{\mathbf{R}}_U} \left[\frac{e^{-jk_0 d}}{C_n^{+(v)}} \left(e^{jk_0 d C_n^{+(v)}} - 1 \right) \right.$$
$$\left. + \frac{e^{+jk_0 d}}{C_n^{-(v)}} \left(e^{-jk_0 d C_n^{-(v)}} - 1 \right) \right] \quad (21)$$

$$C_j^{\pm(v)} = 1 \pm \sqrt{\varepsilon_r^{(v)}} \sin\theta^{(v)} \cos\phi_j \quad (j = n - 1, n). \quad (22)$$

The fact that (15) and (16) do not include any calculations of integrals reduces the computational burden.

III. NUMERICAL VERIFICATION

Once the current distribution along an antenna arm is determined, the input impedance Z_{in} can be obtained from $V_{\text{in}}/I_{\text{in}}$, where V_{in} and I_{in} are the voltage and current at the input terminals, respectively. The power gain is defined as $G(\theta^{(v)}, \phi) = 4\pi U(\theta^{(v)}, \phi)/P_{\text{in}}$, where P_{in} is the total input power to the antenna and

$$U(\theta^{(v)}, \phi) = \frac{1}{2} \sqrt{\frac{\varepsilon_0 \varepsilon_r^{(v)}}{\mu_0}} R_U^2 \left[|E_\theta^{(v)}|^2 + |E_\phi^{(v)}|^2 \right]. \quad (23)$$

When $\theta = \Theta = 0$, (18) and (19) lead to $C_\theta^{(\text{die})} = \sqrt{\varepsilon_r} C_\theta^{(\text{air})}$ and $C_\phi^{(\text{die})} = \sqrt{\varepsilon_r} C_\phi^{(\text{air})}$ and (20) and (21) lead to $\alpha_j^{(\text{die})} = \alpha_j^{(\text{air})}$ ($j = n-1, n$). Therefore, the ratio of the power gains in the $\pm Z_U$ directions $U(\Theta = 0°, \phi)/U(\theta = 0°, \phi)$ is calculated to be $\varepsilon_r^{1.5}$ using (15) and (16) [3].

A computer program has been written for obtaining the current distribution, input impedance, and power gain. We check the validity of the computer program by comparing the published data of a flat conducting plate bow-tie antenna [12] with those obtained by the program.

Fig. 4(a) shows the input impedance locus of a bow-tie antenna when the length $2L$ is changed. The bow tie approximated by wire elements is fed from its center with a δ-gap generator. The parameters are as follows: wire radius $a = 0.001\lambda_0$, bow-tie angle $2\alpha_{\text{bt}} = 60°$, and relative permittivity $\varepsilon_r = 4.0$. The input impedance is normalized to $152 \ \Omega$. The wire element lengths in terms of the free-space wavelength L_{ele}/λ_0 are given in a table for the corresponding input impedance points. For comparison, the input impedance calculated on the basis of the current-mode MoM by Compton [12] is also shown in Fig. 4(a). It is seen that both results are in good agreement.

Fig. 4(b) shows the normalized power pattern of a bow-tie antenna of $2L = 4\lambda_0$, $2\alpha_{\text{bt}} = 60°$, $\varepsilon_r = 3.83$, and $L_{\text{ele}}/\lambda_0 = 0.1$. The pattern (solid line) is obtained by the present numerical analysis for the dielectric material region. It is clear that the present numerical result agrees with Compton's (dotted line). The critical angle, which is given by $\Theta_c = \sin^{-1} \sqrt{1/\varepsilon_r}$, is $30.7°$.

IV. SPIRAL ANTENNA ANALYSIS

Experimental work [2] shows that a two-arm spiral antenna with a detector successfully operates as a quasi-optical receiver for submillimeter-wave astronomy. The spiral antenna has an

$$C_\theta^{(v)} = \frac{\cos\theta^{(v)} \left[\varepsilon_r^{(v)} \sqrt{\varepsilon_r - \left(\varepsilon_r^{(v)} \sin\theta^{(v)}\right)^2} \cos\theta^{(v)} + \varepsilon_r - \left(\varepsilon_r^{(v)} \sin\theta^{(v)}\right)^2 \right]}{\left(\sqrt{1 - \varepsilon_r^{(v)} \sin^2\theta^{(v)}} + \sqrt{\varepsilon_r - \varepsilon_r^{(v)} \sin^2\theta^{(v)}}\right) \left(\varepsilon_r \sqrt{1 - \varepsilon_r^{(v)} \sin^2\theta^{(v)}} + \sqrt{\varepsilon_r - \varepsilon_r^{(v)} \sin^2\theta^{(v)}}\right)} \quad (18)$$

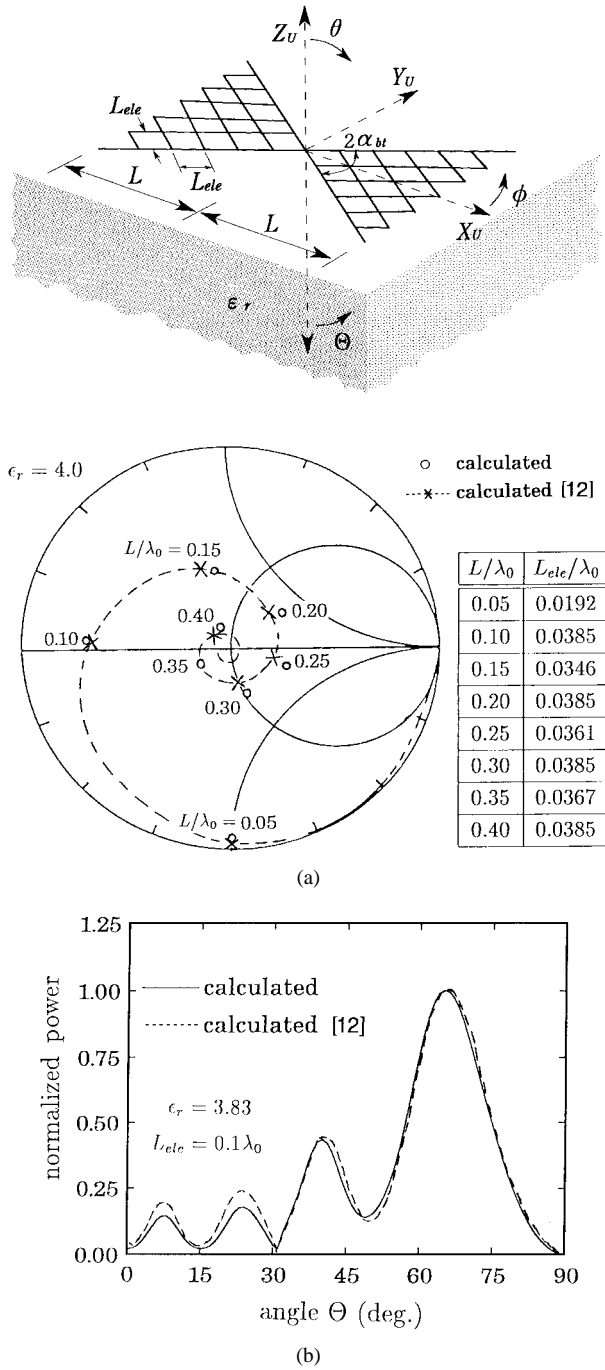| L/λ_0	L_{ele}/λ_0
0.05	0.0192
0.10	0.0385
0.15	0.0346
0.20	0.0385
0.25	0.0361
0.30	0.0385
0.35	0.0367
0.40	0.0385

(a)

(b)

Fig. 4. Bow-tie antenna. (a) Input impedance. (b) Normalized power pattern.

advantage over a bow-tie antenna in that the spiral shows nearly symmetric E- and H-plane patterns with low sidelobes. In this section, the theoretical radiation characteristics of a spiral antenna printed on a semi-infinite dielectric material of relative permittivity ε_r (see Fig. 5) are presented and discussed.

The spiral is Archimedean with feed wires of length e_{st}. The radial distance from the origin (antenna center) to a point on the spiral arm is given by $r_{sp} = a_{sp}\phi_{sp}$, where a_{sp} is the spiral constant and ϕ_{sp} is the winding angle. The antenna parameters are chosen as follows: $e_{st} = 0.04\lambda_0$, $a_{sp} = 0.0153\lambda_0$/rad., 2.6 rad. $\leq \phi_{sp} \leq 36.5$ rad., and wire radius $a = 0.006\lambda_0$. Note that
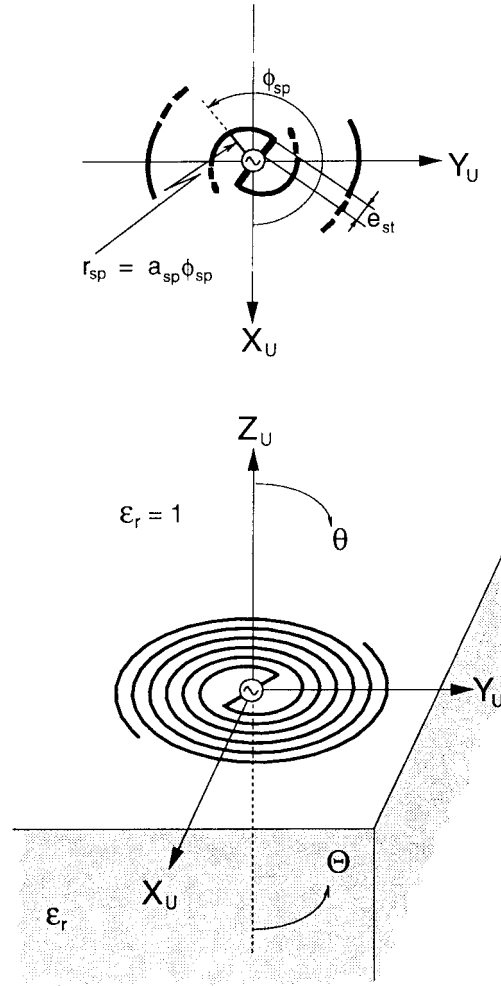

Fig. 5. Two-wire spiral antenna on a semi-infinite dielectric material.

a spiral antenna with $\varepsilon_r = 1$ is used as a reference antenna in the following analysis.

Fig. 6 shows the current distributions and their phase progressions for $\varepsilon_r = 1, 2.55,$ and 12.8. The currents have a traveling wave form. The guided wavelength of each current is close to $\lambda_0/(\varepsilon_{av})^{1/2}$, where ε_{av} is an average relative permittivity for air and the dielectric material: $\varepsilon_{av} = (1 + \varepsilon_r)/2$.

The power patterns are shown in Fig. 7. The critical angles are $\Theta_c = 38.8°$ and $16.2°$ for $\varepsilon_r = 2.55$ and 12.8, respectively. It is clear that, as the relative permittivity ε_r increases, the radiation into the dielectric material becomes stronger in accordance with the $\varepsilon_r^{1.5}$ power gain ratio. Further calculations show that the radiation around the $-Z_U$ axis is circularly polarized. The region over which the radiation is circularly polarized with an axial ratio of less than 3 dB becomes narrower as ε_r increases. This is illustrated in Fig. 8. Since knowing the axial ratios in the dielectric material region is necessary for practical applications such as dielectric hemispherical lenses and earth radar, only the axial ratios in the dielectric material region are shown in Fig. 8.

Fig. 9 shows the frequency response of the power gain in the $-Z_U$ direction. The gains at frequency f_0 (giving a wavelength of λ_0) are approximately 6, 8, and 9 dB for
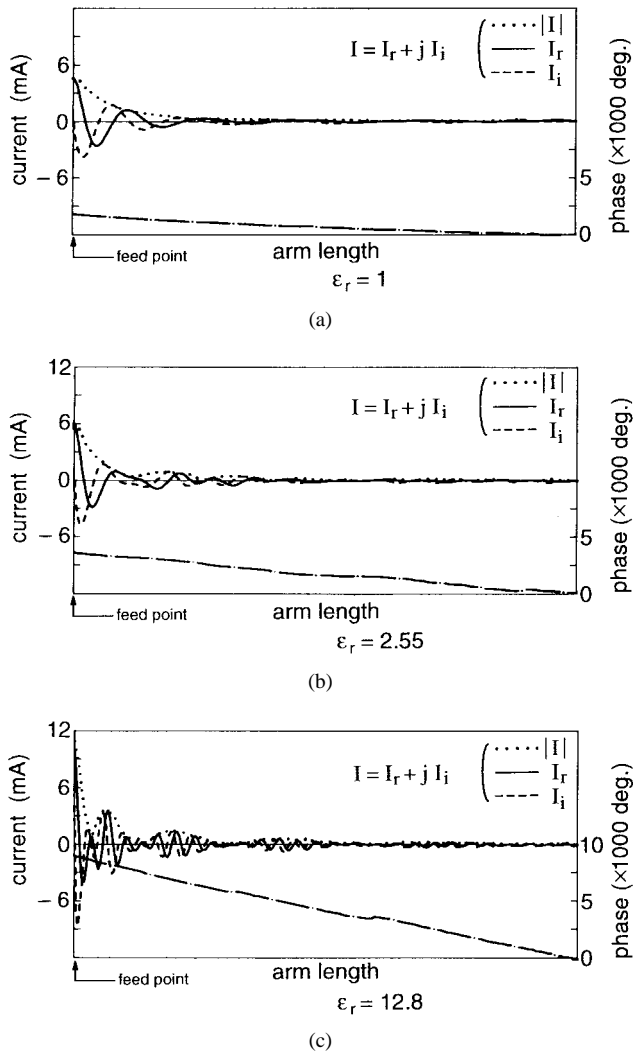
Fig. 6. Current distributions of spiral antennas.

Fig. 7. Power patterns of spiral antennas.

$\varepsilon_r = 1, 2.55$, and 12.8, respectively. It is seen that the gain variation over a frequency range of f_0 to $1.5f_0$ is relatively small.

The frequency response of the input impedance Z_{in} ($= R_{\mathrm{in}} + j X_{\mathrm{in}}$) is shown in Fig. 10. The input impedance is relatively constant by virtue of the traveling-wave current distribution. It is also found that the resistive value of the input impedance decreases as the relative permittivity ε_r increases. Fig. 11 shows the axial ratio in the $-Z_U$ direction versus frequency. It can be said that the spiral's radiation is circularly polarized over a wide frequency range.

V. CONCLUSION

An integral equation for a wire of arbitrary shape on a semi-infinite dielectric material of relative permittivity ε_r is formulated. This equation is characterized by two terms—$\prod_j^{(\mathrm{air})x}$ and $\prod_j^{(\mathrm{air})}$—of Sommerfeld-type integrals. The integral equation is reduced to a set of linear equations $[Z_{m,n}][I_n] = [V_m]$ by the method of moments.

Weighted free-space Green's functions are extracted from $\prod_j^{(\mathrm{air})x}$ and $\prod_j^{(\mathrm{air})}$. The terms $\prod_j^{(\mathrm{air})x}$ and $\prod_j^{(\mathrm{air})}$ after these
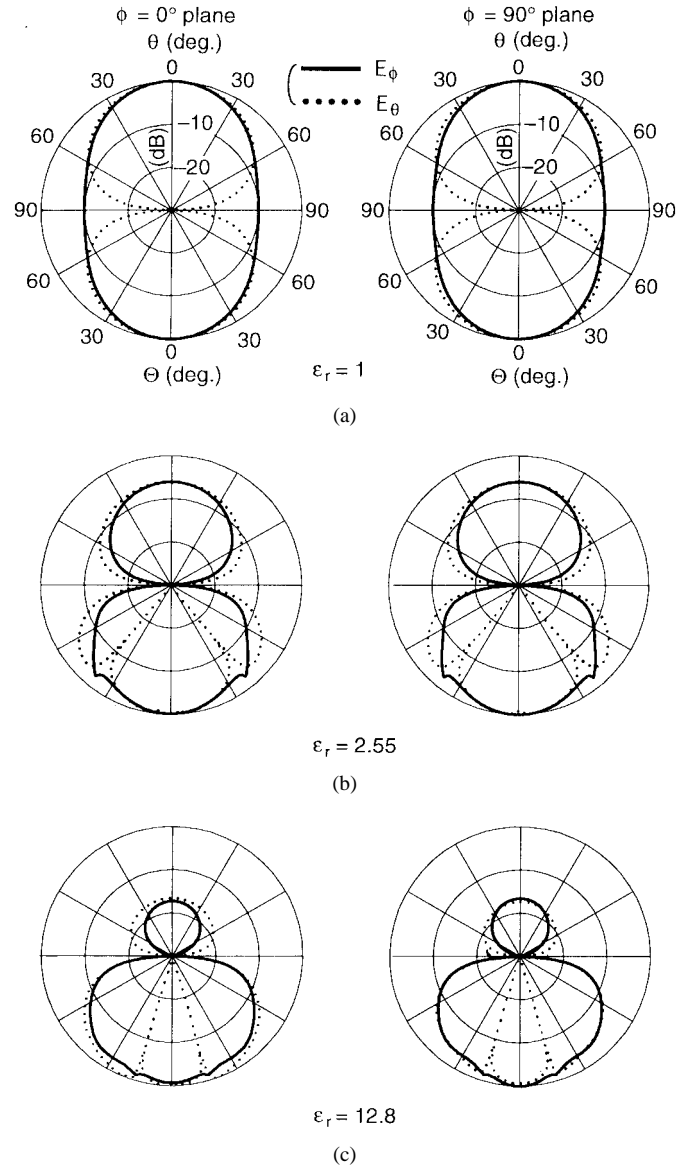
extractions converge rapidly and can be interpolated with respect to the distance between the source and observation points. This interpolation leads to efficient calculation of $Z_{m,n}$.

The far-zone radiation field is also formulated using the stationary phase method. The formulation of the far-zone radiation field does not have any integrals, leading to simple calculations. The field calculation is performed using the expansion function coefficients.

Good agreement is found between the numerical results obtained by the present method and Compton's current-mode moment method for a bow-tie antenna. After the numerical verification with the bow-tie, a two-wire spiral antenna on a semi-infinite dielectric material of permittivity ε_r is numerically analyzed. The numerical results show that the current behaves as a traveling wave with a guided wavelength of approximately $\lambda_g = \lambda_0/\sqrt{(1+\varepsilon_r)/2}$.

Further calculations show that as ε_r increases, the radiation into the dielectric material becomes stronger in accordance with a power gain ratio of $\varepsilon_r^{1.5}$. The axial ratio calculation

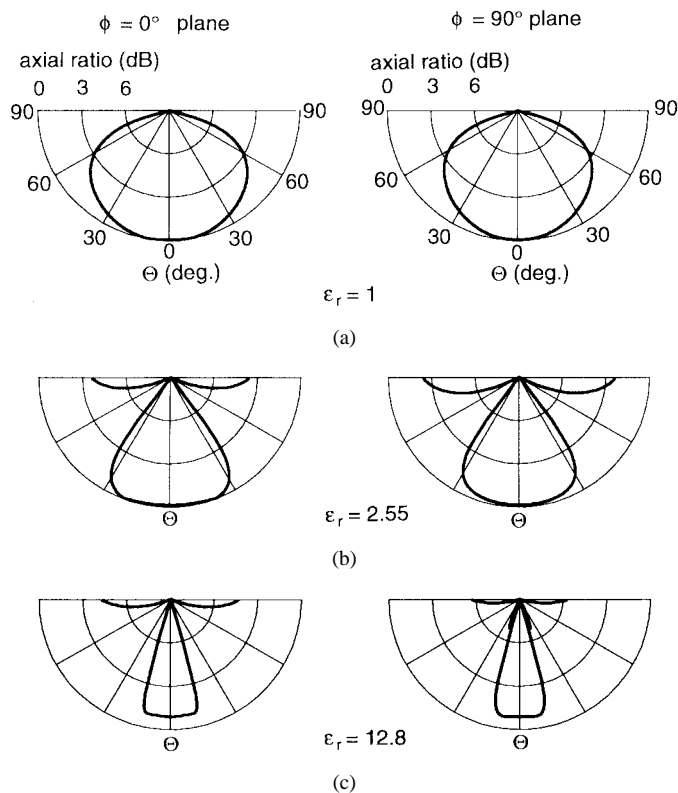$\phi = 0°$ plane $\qquad$ $\phi = 90°$ plane

(a)

(b)

(c)

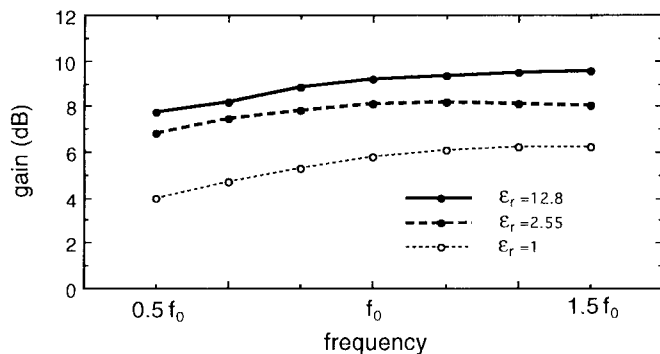Fig. 8. Axial ratios in dielectric materials.

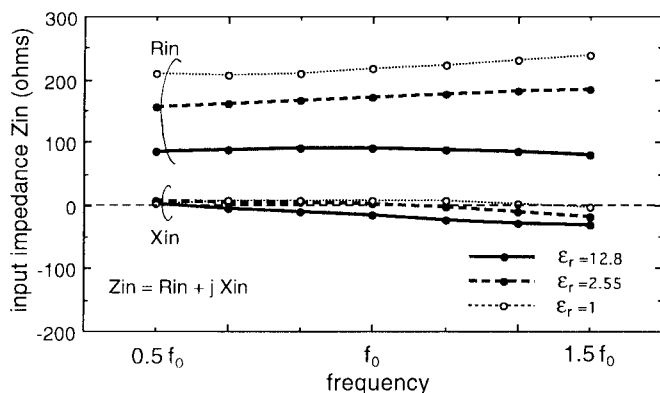Fig. 9. Frequency response of power gain.

Fig. 10. Frequency response of input impedance.

reveals that the spiral radiates a circularly polarized wave around its axis (normal to the spiral plane) in the dielectric
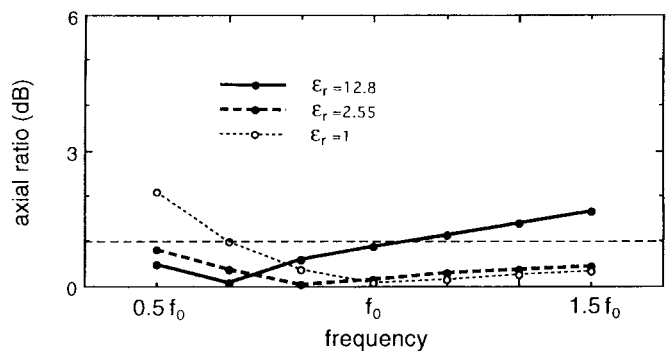

Fig. 11. Frequency response of axial ratio.

material. It is also found that as ε_r increases, the resistive value of the input impedance decreases.

ACKNOWLEDGMENT

The authors would like to thank V. Shkawrytko for his kind discussions.

REFERENCES

[1] D. B. Rutledge and M. S. Muha, "Imaging antenna arrays," *IEEE Trans. Antennas Propagat.*, vol. AP-30, pp. 535–540, July 1982.
[2] T. H. Buttgenbach, R. E. Miller, M. J. Wengler, D. M. Watson, and T. G. Phillips, "A broad-band low-noise SIS receiver for submillimeter astronomy," *IEEE Trans. Microwave Theory Tech.*, vol. 36, pp. 1720–1726, Dec. 1988.
[3] M. Kominami, D. M. Pozar, and D. H. Schaubert, "Dipole and slot elements and arrays on semi-infinite substrates," *IEEE Trans. Antennas Propagat.*, vol. AP-33, pp. 600–607, June 1985.
[4] R. E. Collin and F. J. Zucker, *Antenna Theory*. New York: McGraw-Hill, 1969, Part II, ch. 23.
[5] G. B. Burke and E. K. Miller, "Modeling antennas near to and penetrating a lossy interface," *IEEE Trans. Antennas Propagat.*, vol. AP-32, pp. 1040–1049, Oct. 1984.
[6] K. A. Michalski and D. Zheng, "Electromagnetic scattering and radiation by surfaces of arbitrary shape in layered media—Parts I and II," *IEEE Trans. Antennas Propagat.*, vol. 38, pp. 335–352, Mar. 1990.
[7] D. R. Jackson and N. G. Alexopoulos, "An asymptotic extraction technique for evaluating Sommerfeld-type integrals," *IEEE Trans. Antennas Propagat.*, vol. AP-34, pp. 1467–1470, Dec. 1986.
[8] C. L. Chi and N. G. Alexopoulos, "An image extraction approach to modeling printed circuit antennas," *Electromagn.*, vol. 6, pp. 161–170, 1986.
[9] R. H. Clarke and J. Brown, *Diffraction Theory and Antennas*. New York: Wiley, 1980.
[10] P. B. Katehi and N. G. Alexopoulos, "On the effect of substrate thickness and permittivity on printed circuit dipole properties," *IEEE Trans. Antennas Propagat.*, vol. AP-31, pp. 34–39, Jan. 1983.
[11] H. Nakano, S. R. Kerner, and N. G. Alexopoulos, "The moment method solution for printed wire antennas of arbitrary configuration," *IEEE Trans. Antennas Propagat.*, vol. 36, pp. 1667–1674, Dec. 1988.
[12] R. C. Compton, R. C. McPhedran, Z. Popovic, G. M. Rebeiz, P. P. Tong, and D. B. Rutledge, "Bow-tie antennas on a dielectric half-space: Theory and experiment," *IEEE Trans. Antennas Propagat.*, vol. AP-35, pp. 622–631, June 1987.
[13] H. Nakano and J. Yamauchi, "Characteristics of modified spiral and helical antennas," *Proc. Inst. Elect. Eng.*, vol. 129, pt. H, pp. 232–237, Oct. 1982.
[14] P. E. Mayes, "Planar and other wide-angle logarithmic spirals over ground," *Electromagn.*, vol. 14, pp. 329–362, 1994.
[15] H. Nakano, K. Nogami, S. Arai, H. Mimaki, and J. Yamauchi, "A spiral antenna backed by a conducting plane reflector," *IEEE Trans. Antennas Propagat.*, vol. AP-34, pp. 791–796, June 1986.
[16] J. J. H. Wang and V. K. Tripp, "Design of multioctave spiral-mode microstrip antennas," *IEEE Trans. Antennas Propagat.*, vol. 39, pp. 332–335, Mar. 1991.

[17] S. C. Wu, "Analysis and design of conductor-backed square Archimedean spiral antennas," *Electromagn.*, vol. 14, pp. 305–318, 1994.

[18] C. W. Penney and R. J. Luebbers, "Input impedance, radiation pattern, and radar cross section of spiral antennas using FDTD," *IEEE Trans. Antennas Propagat.*, vol. 42, pp. 1328–1332, Sept. 1994.

[19] K. Hirose and H. Nakano, "Dual-spiral slot antennas," *Proc. Inst. Elect. Eng.*, vol. 138, pt. H, pp. 32–36, Feb. 1991.

[20] N. J. Champagne II, J. T. Williams, and D. R. Wilton, "Analysis of resistively loaded, printed spiral antennas," *Electromagn.*, vol. 14, pp. 363–395, 1994.

Kazuhide Hirose (M'92) was born in Kanagawa, Japan, on September 18, 1959. He received the B.E., M.E., and Dr.E. degrees, all from Hosei University, Tokyo, Japan, in 1982, 1984, and 1991, respectively.

From 1984 to 1987, he was with Nihon Dengyo Kosaku Co., Ltd., Antenna Division, Tokyo, Japan. From 1991 to 1995, he was a Lecturer at Shonan Institute of Technology, Kanagawa, Japan. Since 1995 he has been a Faculty Member of Tokyo Denki University, Saitama, Japan, where he is an Associate Professor of electrical engineering. His research interests include printed antennas and slot antennas.

Dr. Hirose is a member of the Institute of Electronics, Information, and Communication Engineers of Japan.

Hisamatsu Nakano (M'75–SM'87–F'92) was born in Ibaraki, Japan, on April 13, 1945. He received the B.E., M.E., and Dr.E. degrees in electrical engineering all from Hosei University, Tokyo, Japan, in 1968, 1970, and 1974, respectively.

Since 1973, he has been a member of the faculty of Hosei University, Tokyo, Japan, where he is now a Professor of electronic informatics. He was a Visiting Associate Professor at Syracuse University, Syracuse, NY (March–September 1981), where he worked on numerical analysis of electromagnetic coupling between wires and slots. He was also a Visiting Professor at the University of Manitoba, Canada (March–September 1986), researching numerical techniques for analysis of microstrip antennas, and a Visiting Professor at the University of California, Los Angeles (September 1986–March 1987), working on microstrip line antenna analysis. He has developed a parabolic antenna using a backfire helical feed for direct reception of the broadcasting satellite TV programs (DBS). He has also developed two types of small indoor flat DBS antennas using novel elements: curled and extremely low-profile helical elements. His other developments include microstrip antennas for global positioning systems (GPS), personal handy telephone antennas, and small dual-polarization Cassegrain antennas for direct reception of communication satellite TV programs. He has published more than 120 refereed journal papers and 80 international symposium papers on antenna and relevant problems. He is the author of *Helical and Spiral Antennas* (New York: Wiley, 1987). He also published the chapter "Antenna analysis using integral equations," in the *Analysis Methods of Electromagnetic Wave Problems—Volume II* (Norwood, MA: Artech, 1996). His research topics include numerical methods for antennas, electromagnetic wave scattering problems, and light-wave problems.

Dr. Nakano was the recipient of an International Scientific Exchange Award from the Natural Sciences and Engineering Research Council of Canada in 1986. In 1987, he received the Best Paper Award of Institute of Electrical Engineers Fifth International Conference on Antennas and Propagation. In 1994, he received the IEEE AP-S Wheeler Award for best paper. He is an Associate Editor of *IEEE Antennas and Propagation Magazine*

Ichiro Oshima was born in Tochigi, Japan, on January 13, 1970. He received the B.E. and M.E. degrees from Hosei University, Tokyo, Japan, in 1993 and 1995, respectively.

He joined the Denki Kogyo Co., Ltd., Tokyo in 1995.

Mr. Oshima is a member of the Institute of Electronics, Information, and Communication Engineers of Japan.

Junji Yamauchi (M'85) was born in Nagoya, Japan, on August 23, 1953. He received the B.E., M.E., and Dr.E. degrees, all from Hosei University, Tokyo, Japan, in 1976, 1978, and 1982, respectively.

From 1984 to 1988, he served as a Lecturer at the Electrical Engineering Department of Tokyo Metropolitan Technical College, Japan. Since 1988 he has been a Faculty Member of Hosei University, where he is now a Professor of electronic informatics. His research interests include circularly polarized antennas and optical waveguides.

Dr. Yamauchi is a member of the Optical Society of America and the Institute of Electronics, Information, and Communication Engineers of Japan.